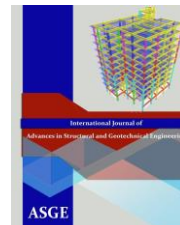# Behavior of Arched Self-Compacted Perforated Reinforced Concrete Beams

Salah El-Din F. Taher[1], Hamdy M. Afefy[2], Nesreen M. Kassem[3], Mohammed Salah El-Sensar[4]

[1]*Professor of Concrete Structures, Structural Engineering Dept., Faculty of Engineering, Tanta University, Tanta, Egypt*
E-mail: salah.taher@f-eng.tanta.edu.eg

[2]*Professor of Concrete Structures and Head of Construction Engineering and Management Department, Pharos University in Alexandria, Egypt. On leave from Tanta University*
E-mail: hamdy.afefy@pua.edu.eg and hamdy.afefy@f-eng.tanta.edu.eg

[3]*Associate Professor, Structural Engineering Dept., Faculty of Engineering, Tanta University, Tanta, Egypt*
E-mail: nesreen.kassem@f-eng.tanta.edu.eg

[4]*Master Student, Structural Engineering Dept., Faculty of Engineering, Tanta University, Tanta, Egypt.*
E-mail: PG_80071@f-eng.tanta.edu.eg

ABSTRACT

Providing web openings in reinforced concrete (RC) beams facilitates passing the pipes and ducts of utility services as well as it has a good-looking appearance when arranged in regular module. The current paper presents both experimental and numerical investigations on the overall structural performance of two-hinged perforated self-compacted RC arched beams. Three main factors were studied; namely, the percentage of mass loss (9% 16% and 29%) due to the provided perforations, the effect of the curvature ratio and the perforations shape (circular, oval, and square). Therefore, three perforation sizes were studied having perforation diameter to the beam total depth ratio (D/t) of 0.33, 0.50, and 0.67. Accordingly, five perforated arched beams, one solid reference arched beam and one solid straight beam were prepared and configured then tested under concentrated loading till complete collapse. Besides, numerical validation using ABAQUS program has been conducted on the perforated arched beams. It was found that the ached beam showed remarkable ultimate capacity compared to that of straight beam; however the strength gain due to arching effect reduce significantly based on the perforation size and shape. Furthermore, the obtained responses along with the mode of failure from the experimental test were compared with the predicted ones from the numerical simulation. Comparison showed good agreement between the displayed mode of failure, ultimate capacity and the developed mid-span deflection obtained from both numerical simulation and the experimental tests.

Keywords: Arched beam, Perforated beam, ABAQUS software, Finite Element Method, Self-compacted concrete (SCC)

1. INTRODUCTION

Nowadays, providing web openings in the reinforced concrete beams in modern reinforced concrete structures became a common practice [1]. These openings are necessary for passing ducts and piping for different service facilities such as air conditioning, sewages water supply and computer networks. On the other hand, these openings interrupt the loading trajectories

and may defect the structural performance of the beam due to the presence of the weak points around the openings [2]. Moreover, irregular locations of such openings can impair the aesthetic appearance of the beam. Therefore, choosing the accurate location of such openings is an important issue as well as providing necessary reinforcement around the opening should be arranged in order to prevent any premature failure of the beam containing web openings [1,3].The majority of performed studies investigated the flexural and shear behavior of RC beams with a single opening in the entire span or an opening in each half-span as opposed to the present study, which considered RC beams with multiple discrete openings.

The provided openings in RC beams may take any shape, however, the circular and the rectangular configurations are the most common shapes [4, 5]. The web opening could be classified as small or large opening based on either the size of opening and/or the overall structural performance of the beam containing the openings. However, there is no distinction limit between the small and large openings classification. Mansur [6] differentiated between two different shear failure modes of an RC beam containing a small opening. In beam-type shear failure, the failure plane formed by the diagonal crack passes through the center of the opening. In frame-type failure, two separate diagonal cracks form in the top and bottom chord members above and below the opening are formed as shown in Fig.1.
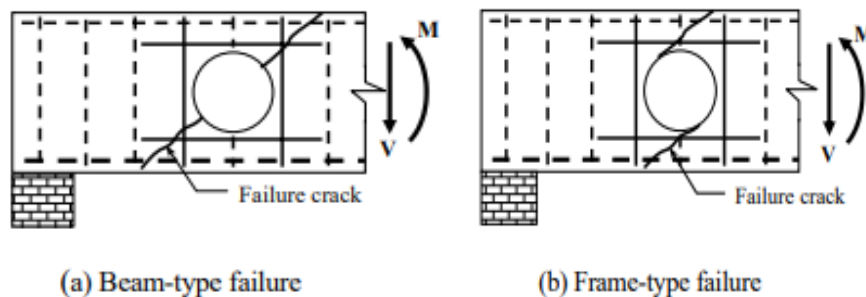

(a) Beam-type failure   (b) Frame-type failure

Fig. 1 Modes of failure for small and large openings.

The experiments indicated that the use of diagonal reinforcement is an effective method in crack control of RC beams with openings and the shear forces in a beam are distributed to the chord members in proportion to their cross-sectional areas as suggested by [6]. Al Sheikh [7] studied the flexural behavior of RC beams with circular, square and rectangular openings. It was concluded that the most favorable behavior was for circular single opening where the maximum reductions on the ultimate capacity were about 1.5% and 10% for small and large opening, respectively. Aykac and Yilmaz [8] tested RC beams with regular triangular or circular openings. The beams with circular openings were found to have a more ductile flexural behavior compared to the ones with triangular openings. The influence of web openings on the ductility and load-carrying capacity of a beam was shown to increase with the increasing tensile reinforcement ratio in the beam. Furthermore, it was found that introducing large opening without providing proper internal reinforcement could reduce the ultimate capacity significantly [9]. However, providing sufficient diagonal reinforcement around the openings eliminated shear failure of the web posts and prevented premature failure of the beam [10]. Providing multiple web opening in RC beams have been studied recently considering different shapes such as circular, oval, square and rectangle and hexagonal. It was found that reinforcement configuration around the openings and the opening size are the governing factor on the ultimate capacity of such perforated beams [11-15].

In the current study, a new perforated two-hinged arched beam system is developed and tested under concentrated central loading. In order to facilitate casting the concrete around the openings (perforations) and preventing any honeycomb, self-compacted concrete was selectively chosen. Accordingly, five perforated arched beams, one solid arched beam and one straight solid self-compacted RC beams were cast and tested in order to verify their flexural resistance under concentrated loading. The effect of the mass loss due to the provided perforations (9%, 16% and 29%), which corresponds to perforations diameters of 100, 150 and 200 mm, respectively, and the perforations shape (circular, square and oval) were the main studied parameters. Numerical analysis using ABAQUS software [16] was used to verify the numerical simulation of the perforated arched beam.

2. EXPERIMENTAL WORK PROGRAM

2.1 Test specimens

A total of seven beams were tested in this paper; five perforated arched beams as well as one solid reference arched beam and straight solid beam were prepared and configured as summarized in Table 1. All arched beams and straight beam had the same cross-sectional dimensions of 150 mm width by 300 mm total depth. The span of the arched beams and straight beam center-to-center was 2210 mm. The flexural reinforcement of all beams consisted of two deformed steel bars of 16 mm diameter in the tension side and two deformed steel bars of 12 mm diameter in the compression side, in order to ensure tension failure of the beams. The stirrups of the solid arched and straight beam consisted of smooth bars of 8 mm diameter spaced every 100 mm along the entire span of the beam.

Table 1 Test matrix

Specimen	D/t	Mass loss, %	Characteristics	Objective
BSC	NA	0.00	Straight control beam	Studying the effect of curvature
BCS-C-R60	NA	0.00	Curved control beam	
BCP-D10-R60	0.33	9%	Curved beam having perforation diameter of 100,150 and 200 mm, rise = 600 mm	Studying the effect of changing the perforations size
BCP-D15-R60	0.5	16%		
BCP-D20-R60	0.67	29%		
BCP-B15-R60	0.5	21%	Curved perforated beam with square and oval openings	Studying the effect of changing the perforations shape
BCP-O10/20-R60	0.67	20%		

D/t = the perforation depth to the overall depth of the beam.

In addition to the control straight and arched solid beam, five perforated beams were configured as illustrated herein below. One arched beam (BCP-D10-R60) having rise of 60 mm was provided by circular perforations of 100 mm diameter (D/t = 0.33) spaced every 300 mm while the width of the web posts between the perforations was 150 mm which is higher than one half of the perforation diameter in order to ensure that each perforation behaves independently. In addition, in order to avoid shear failure near the supports, solid parts of lengths more than one-half of the beam's depth was provided at both ends. For the arched beam having perforations size of 100 mm diameter, the percentage of mass loss was about 9%. Another arched beam (BCP-D15-R60) with rise of 60 mm was provided by circular perforations of 150 mm diameter (D/t = 0.50) spaced every 300 mm Hence, the percentage of the mass loss for such perforations size was about 16%. Also, one arched beam (BCP-B15-R60) was provided by square perforations of 150 mm (D/t = 0.5) spaced every 300 mm while the width of the web posts between the perforations was 150 mm. For the arched beam having square perforations size of 150 mm, the percentage of mass loss was about 21%. Furthermore, one arched beam (BCP-D20-R60) was provided by circular perforations of 200 mm diameter (D/t = 0.67) spaced every 300 mm while the percentage of mass loss was about 29%. Finally, one arched beam having oval perforations of 200 mm and 100 mm long and short diameters (BCP-O10/20-R60) spaced every 200 mm was prepared and configured to have a mass loss of about 20%. Fig 2 shows the concrete dimensions as well as the perforations layout for all perforated arched beams and actual reinforcement detailing around the perforations for arched beams. In order to form the circular perforations, PVC pipes of 100, 150 and 200mm diameter having 2 mm thickness were cut into slices of 150 mm depth and fixed accurately in the wooden form as shown in Fig. 3. As for oval perforations, two adjacent PVC pipes of 100 mm diameters were used as depicted in Fig. 3. The internal steel cages for straight and arched beams are depicted in Fig. 4.
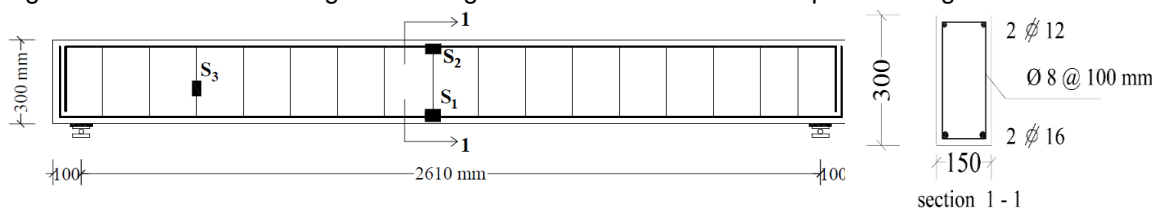

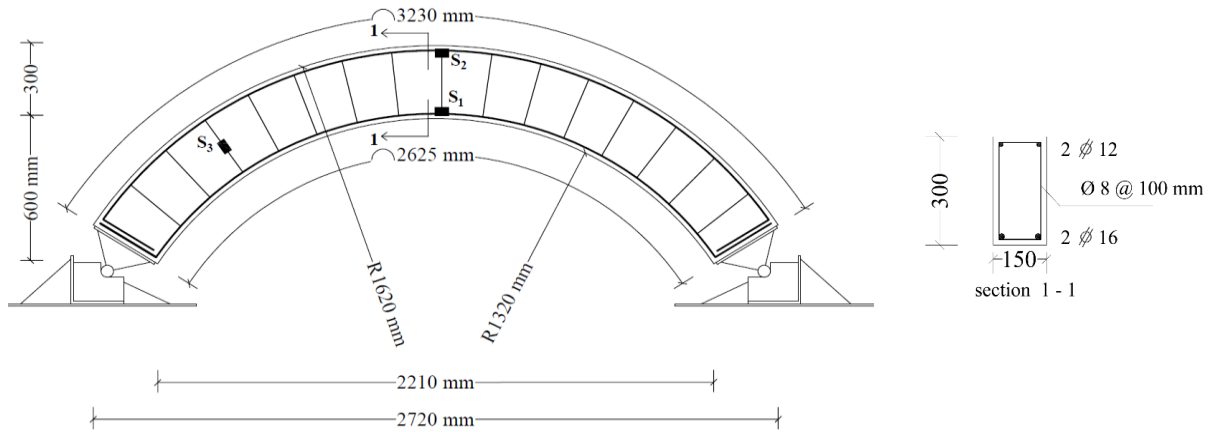**Fig. 2(a) Concrete dimensions and reinforcement detailing for BSC.**

Fig. 2(b) Concrete dimensions and reinforcement detailing for BCS-C.
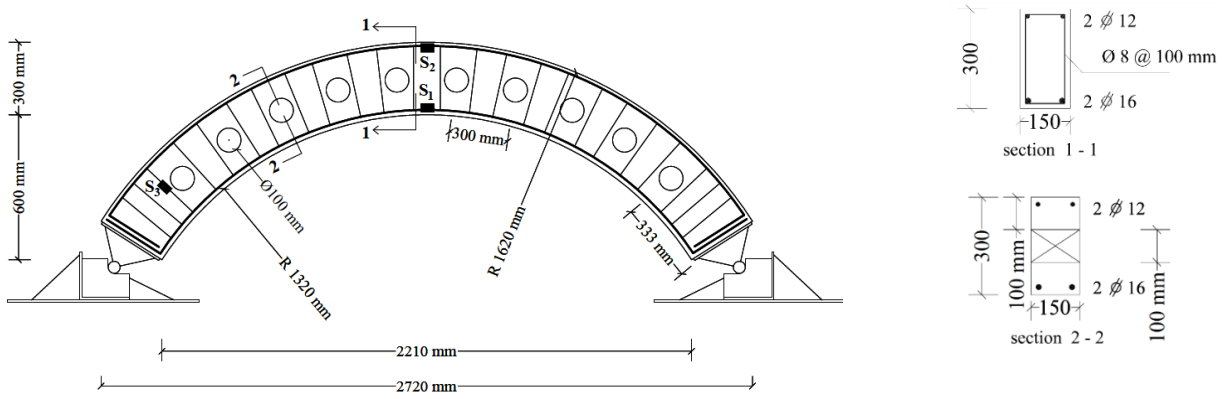
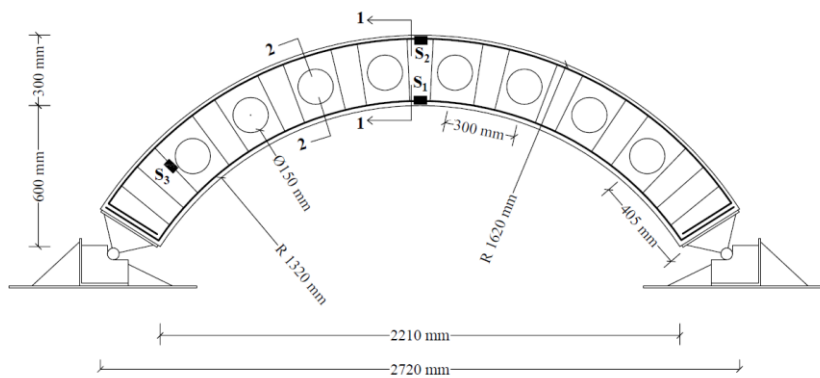**Fig. 2(c) Concrete dimensions and reinforcement detailing for BCP-D10-R60.**

Fig. 2(d) Concrete dimensions and reinforcement detailing for BCP-D15-R60.
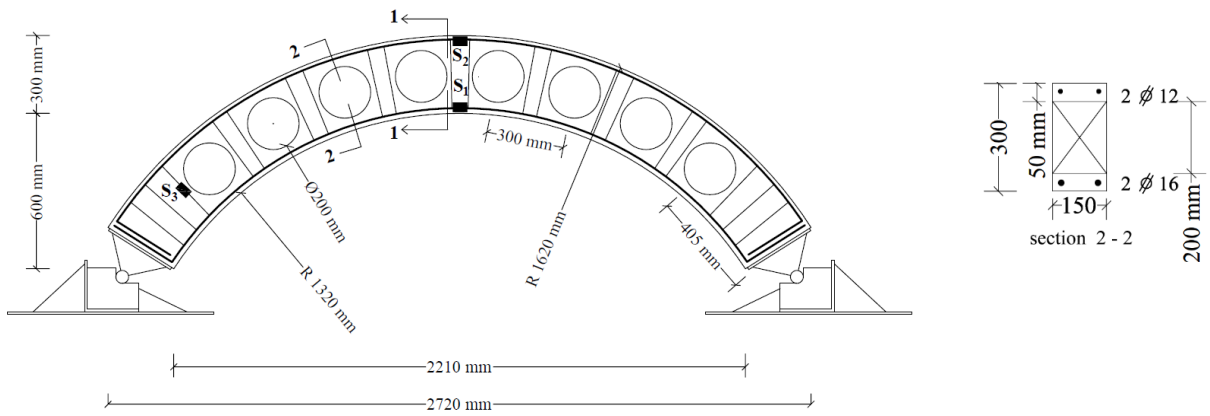
Fig. 2(e) Concrete dimensions and reinforcement detailing for BCP-D20-R60.
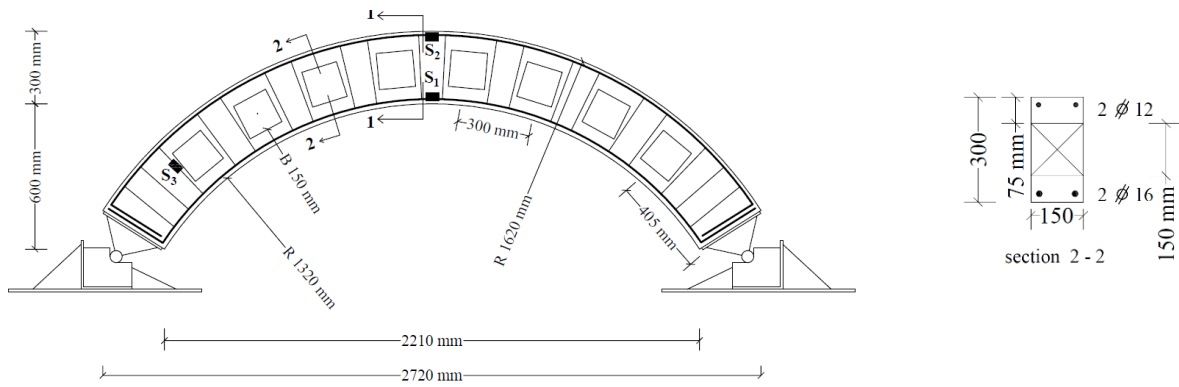
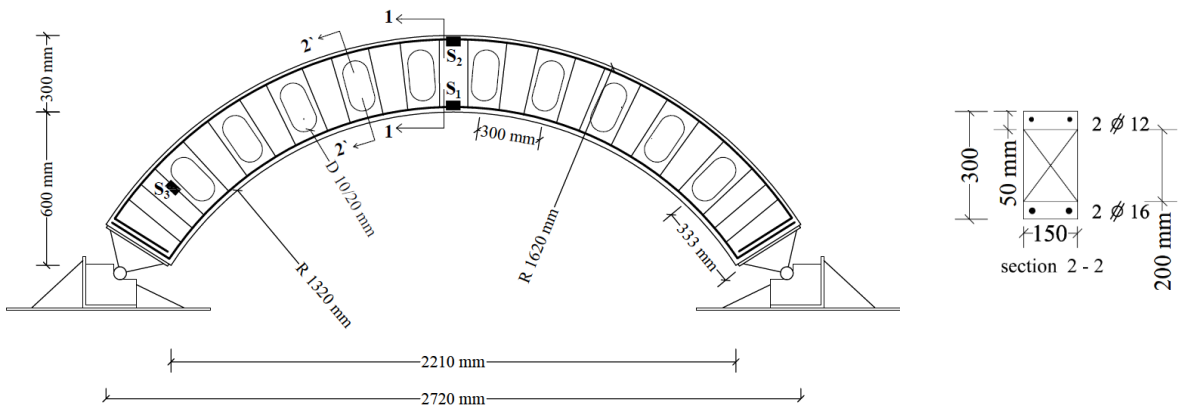**Fig. 2(f) Concrete dimensions and reinforcement detailing for BCP-B15-R60.**

Fig. 2(g) Concrete dimensions and reinforcement detailing for BCP-O10/20-R60.

Fig. 3 Formwork used for casting BSS, BCS-C-R60, BCP-D10-R60, BCP-D20-R60, BCP-D15-R60, BCP-B15-R60 and BCP-O10/20-R60.

Fig. 4(a) Reinforcing steel cage of BSC.

Fig. 4(b) Reinforcing steel cage of BCP-D15-R60.

Fig. 4(c) Reinforcing steel cage of BCP-D10-R60.

Fig. 4(d) Reinforcing steel cage of BCS-C-R60.

Fig. 4(e) Reinforcing steel cage of BCP-D20-R60.

2.2 Material properties

In order to facilitate pouring the concrete around the perforations, self-compacted concrete (SCC) has been selectively chosen. The SCC material consists of ordinary Portland cement.

natural sand. Silica fume super plasticizer .and clean water. The proportion for SCC mix in one cubic meter is presented in Table 2.

Table 2 Mix proportions for casting one cubic meter (1m^3) of SCC

Concrete Mix	W/B	cement	Sand	Coarse aggregates	Water	Silica fume	Super-Plasticizer
SCC	0.41	400	800	930	180	40	4.8

W/B is the water / binder ratio, B = cement + silica fume, Super-plasticizer = 1.2% liter by weight of cement

The fresh SCC is characterized by filling, passing and segregation resistance ability. Different test methods have been used in order to verify such abilities. In the current study, the filling ability was assessed using slump flow test, while the passing ability was determined by the L-box test and segregation resistance was tested with the V-funnel test. For the slump test, the average diameter of the concrete circle was about 630 mm and the time T50cm was about 3 sec. which confirmed with different specifications of SSC [17,18]. The ratio (H2/H1) according to L-box test corresponding to the ratio between the height of the concrete at the end of the horizontal section and the total height was about 0.85, which confirmed with different specifications of SSC [17–20]. As for the V-funnel test, the time for the fresh concrete to flow through the apparatus was about 6 sec., while the time T5 mins that indicates the tendency for segregation of fresh concrete left for 5 min to settle and then used to fill the V-funnel was about 10 sec. The results of the V-funnel test were confirmed with different specifications of SSC [17,18]. Fig. 5 shows the test results of both slump test and L-box test. For hardened concrete, the actual compressive strength was calculated as the average value of six pre-prepared standard cubes of 150 mm side length that were collected from different locations at the casting day. The average compressive strength was about 45 MPa, which corresponds to all beams where testing of all beams was done in two consecutive days.

Fig. 5 Flow ability of the used self-compacted concrete.

As for the longitudinal steel bars as well as the stirrups, in order to determine the mechanical properties, tensile tests were performed on three specimens for each bar size. Table 3 summarizes the mean values of tensile yield strength, ultimate strength and Young's modulus for each bar size.

Table 3 Mechanical properties of the used steel bars

Bar diameter, mm	Type	Average yield strength, MPa	Average tensile strength, MPa	Average modulus of elasticity, GPa
16	Deformed	425	570	204
12	Deformed	430	590	205
8	Smooth	280	420	200

2.3 Test setup

The experimental program has been carried out at the reinforced concrete laboratory of the Faculty of Engineering, Tanta University, Egypt. In order to measure the deformed shapes of all beams, three LVDTs having 100 mm gauge length were used as shown in Fig. 6. The developed normal strains on the tensile steel bars were measure by strain gauges of 6 mm gauge length. In addition, the developed strains on the concrete surface were measured by 100 mm Pi-gauges. The specimen ends were simply-supported over hinged support at both ends by an inclination angle of 32 degrees. Arched beams were loaded by one concentrated load in the mid-span point. The arched beams were loaded incrementally under static loading up to complete collapse. The load on the arched beams was measured by a load cell of 600 kN capacity. After each loading step, the vertical deflections along the measuring points, the developed normal strains in the steel bars as well as the developed strains on the concrete surface were recorded and stored by an automatic data logger unit (TDS-150).
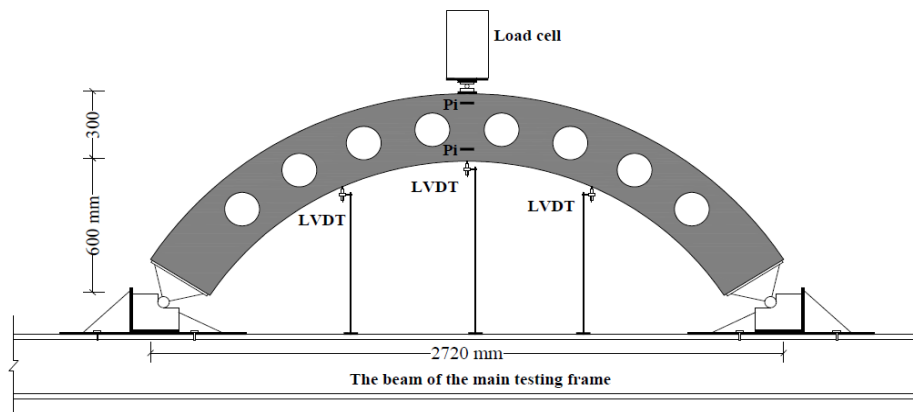

Fig. 6 Test setup.

3. EXPERIMENTAL TEST RESULTS

Based on the adopted reinforcement configuration, the straight solid beam developed regular flexural failure near the mid-span section, while the solid arched beam failed due to shear. Besides, near failure the solid arched beam exhibited horizontal cracks near the mid-span section as result of the restrained ends as well as the developed normal force. On the other hand, all arched beams started to show flexural cracks at the middle part of the span and with further loading, flexural cracks began to be distributed around the middle part and increased in their lengths and widths. In the sequel, flexural shear cracks were developed and finally shear cracks were formed. Subsequently, all perforated arched beams were failed due to frame-type shear mode except beam BCP-D10-R60, which failed due to beam-type shear mode as depicted in Fig.7. Table 4 summarizes the experimental loads at different stages for all beams.

BSS
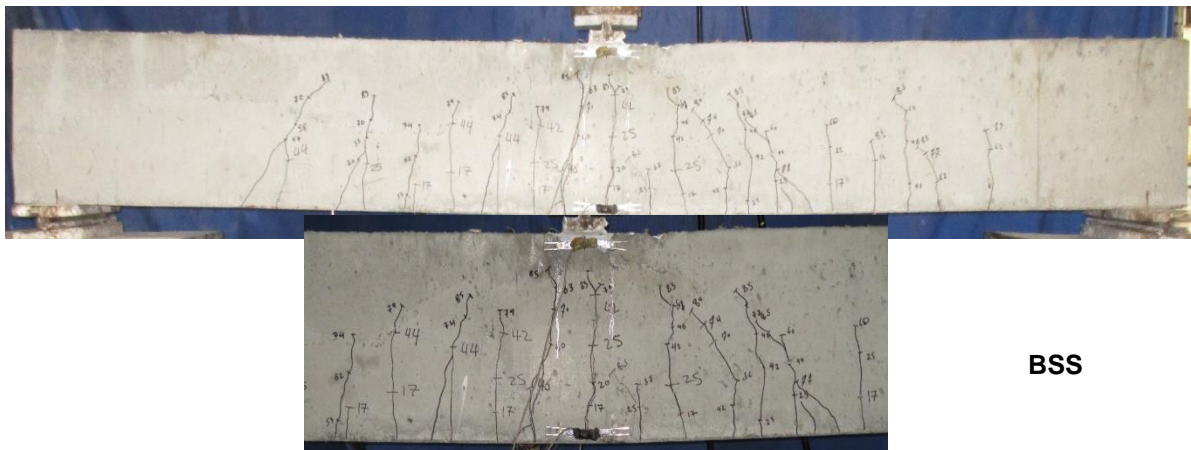
BCSC

BCP-D10-R60

BCP-D15-R60

BCP-D20-R60

BCP-O10/20-R60

BCP-B15-R60

Fig. 7 Crack patterns of all tested beams after complete failure.

Table 4 Experiment results of straight beam and the arched beams.

specimens	First flexural cracking load, kN	First shear cracking load, kN	The ultimate load, kN
BSS	17	42	89
BCS-C-R60	37	44	480
BCP-D10-R60	46	99	451
BCP-D15-R60	26	65	187
BCP-D20-R60	15	35	91
BCP-B15-R60	6	18	119
BCP-O10/20-R60	4	24	58

For straight solid beam, the first flexural crack started to appear at the mid-span section of the beam at a vertical load of about 17 kN. Proceeding with loading, the flexural cracks spread at the tension side till a vertical load of about 42 kN, and then shear cracks began to appear. Soon later the beam was no longer sustained more loading and the beam reached complete tensile flexural failure at a vertical load of about 89 kN. On the other hand, the curved solid beam started to develop flexural crack at the mid span section at a vertical load of about 37 kN, which is more than twice the corresponding one in the straight beam. Soon later, it showed shear cracking at a vertical load of about 44 kN that was close to the opponent one on the straight beam. With further loading, the flexural cracks spread at the tension side till a sudden local shear crack appeared in the upper chord and the beam reached failure at a vertical load of 480 KN.

For curved beam having circular opening of diameter 100 mm (D/t=0.33), flexural cracks started to be developed at the mid span section at a vertical load of about 46 kN, while, the first cracking due to shear started to appear at a vertical load of about 99 KN. With further loading, the flexural cracks spread at the tension side till a sudden local shear crack appeared in the upper chord and the beam reached failure at a vertical load of 451 kN. Increasing the opening diameter to 150 mm (D/t=0.5) resulted in decrease the gained enhancement due to the arching action where the ultimate load reach about twice the ultimate load of the straight beam. Increasing the opening diameter further to 200 mm (D/t=0.67) resulted to exploit all the strength gain where the ultimate capacity reached approximately the corresponding capacity of the straight beam.

It can be observed that increasing the opening diameter provided in the arch beams resulted in accelerated the appearance of cracks due to shear stresses compare to those of the solid arched beam. In addition, increasing the opening diameter has shown more decrease in the ultimate load carrying capacity compared with that of solid arched beam.

For curved beam having square opening of side length of 150 mm (D/t=0.5), flexural cracks started to develop at the mid span section at a vertical load of about 6 kN, while, the first cracking due to shear started to appear at a vertical load of about 18 KN. With further loading, the flexural cracks spread at the tension side till a sudden local shear crack occured in the upper chord and the beam reached failure at a vertical load of 119 KN.

For curved beam having oval opening of diameter 100/200 mm, flexural cracks started to develop at the mid span section at a vertical load of about 4 kN, while, the first cracking due to shear started to appear at a vertical load of about 24 KN. With further loading, the flexural cracks spread at the tension side till a sudden local shear crack occurred in the upper chord and the beam reached failure at a vertical load of 58 KN.

4. FINITE ELEMENT MODELING

In this part, the adopted failure criteria of both concrete and reinforcing steel bars were explained along with their behavior in tension and compression. Besides, the elements representation was outlined for both concrete and reinforcing steel. Finally, a verification of the modeling parameters was conducted by comparing the resulting response of already tested beam with the results of the numerical simulation for tested beams.

In this paper concrete damage plasticity model was chosen to model the concrete behavior. This model assumes that the main two failure modes are tensile cracking and compressive crushing as will be illustrated herein below.

4.1 Uniaxial tension behavior of concrete

Concrete behaves linearly elastic in the first stage of its tensile behavior. In this stage the tensile stress , f_{ct}, is linearly proportionate the tensile strain through elastic modulus, E_c, [21] as shown in Fig.2.

$$E_c = 4400\sqrt{f_{cu}} \qquad \text{(MPa)} \qquad\qquad (1)$$

$$f_{ct} = 0.6\sqrt{f_{cu}} \qquad \text{(MPa)} \qquad\qquad (2)$$

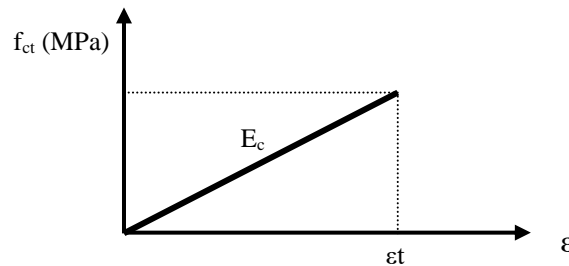Where f_{cu} = concrete compressive cubic strength.

Fig. 8 Stress-strain relationship under uni-axial tension up to first cracking load.

In the second stage; tension softening starts where micro cracks grow to macro cracks and stiffness significantly decreases to zero. Tension softening is defined by stress-strain or stress-displacement relationships and to specify the post-peak tension failure behavior of concrete, the fracture energy method was used. The fracture energy can be estimated by the following equation proposed by Hillerborg [22] as depicted in Fig.9:

$$G_f = 110\left(\frac{f_{cy}}{10}\right)^{0.18} \quad \text{Jole/m}^2 \qquad\qquad (3)$$

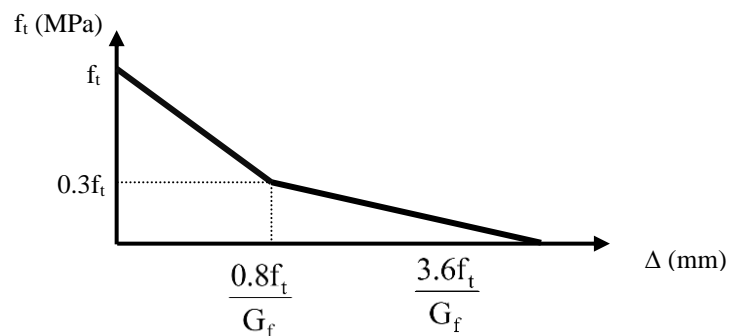Where G_f = fracture energy; f_{cy} = concrete cylindrical compressive strength

Fig. 9 Post-peak stress deformation relationship under uniaxial tension.

4.2 Uniaxial compressive behavior of concrete

For the compression stress-strain curve of the concrete, the stress–strain relationship proposed by Park and Paulay [23] was used to construct the uni-axial compressive stress–strain curve for

concrete as shown in Fig.10 and illustrated by Eq. (4) and (5). Poisson's ratio was assumed to be 0.22

when $\quad \varepsilon \leq 0.002,$ $\qquad f_c = f_c ' \left[2 \frac{\varepsilon_c}{\varepsilon_0} - \left(\frac{\varepsilon_c}{\varepsilon_0} \right)^2 \right]$ $\qquad$ (4)

when $\quad 0.002 \leq \varepsilon \leq 0.0035,$ $\qquad f_c = f_c ' \left[1 - 0.15 \frac{\varepsilon - \varepsilon_0}{\varepsilon_{cu} - \varepsilon_0} \right]$ $\qquad$ (5)
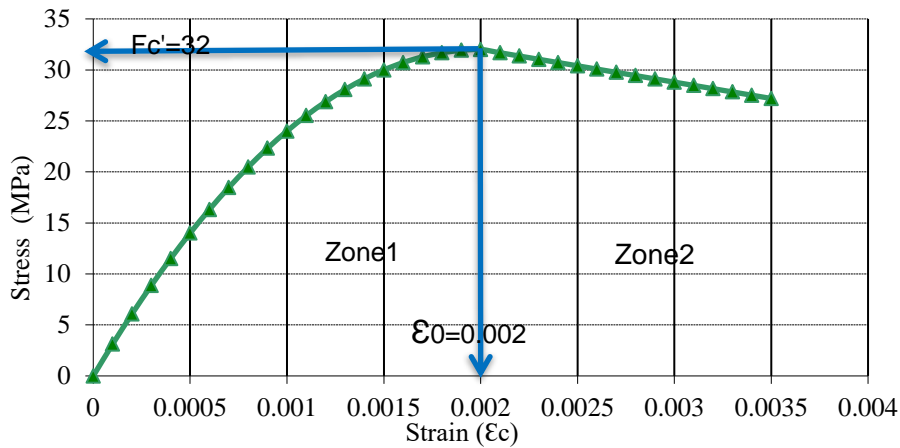

Fig. 10 Schematic diagram of adopted concrete stress-strain behavior in compression.

4.3 Steel reinforcement

The behavior of reinforcing steel bars was assumed to be bilinear elasto–plastic material and identical in tension and compression as depicted in Fig.11. Elastic behavior of steel material is defined by specifying Young's modulus (E_s) and Poisson's ratio (v) of which typical values are 2 x 10^5 MPa and 0.3, respectively. The bond between steel reinforcement and concrete was assumed to be perfect bond.
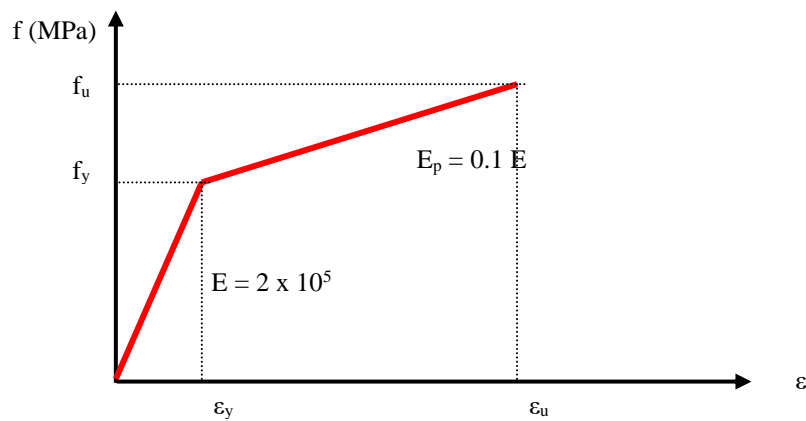

Fig. 11 Idealized stress-strain curve for steel reinforcement.

4.4 Finite element mesh

8-node three-dimensional linear brick, reduced integration, hourglass control element, namely C3D8R, was used for representing concrete. The solid 8-node element (C3D8R) activates the three translational degrees of freedom at each nodes u, v, and w in x, y, and z directions. On the other hand, A 2-node linear three-dimensional truss element namely T3D2 was used for steel embedded in concrete tension and compression zones as well as the internal

trusses. There are three translational degrees of freedom at each of nodes of (T3D2) truss elements u, v, w in x, y, and z directions.

5. COMPARSION BETWEEN NUMERICAL AND EXPERIMENTAL RESULTS

In order to investigate the efficiency of numerical simulation, the exhibited failure modes as well as the numerical load-deflection responses were compared with those mapped and measured during testing of all beams. Comparison showed good agreement between the manifested modes of failure, the ultimate capacity and the developed mid-span deflection relationship obtained from both numerical simulation and the experimental tests as depicted in Figs 12 to 14.
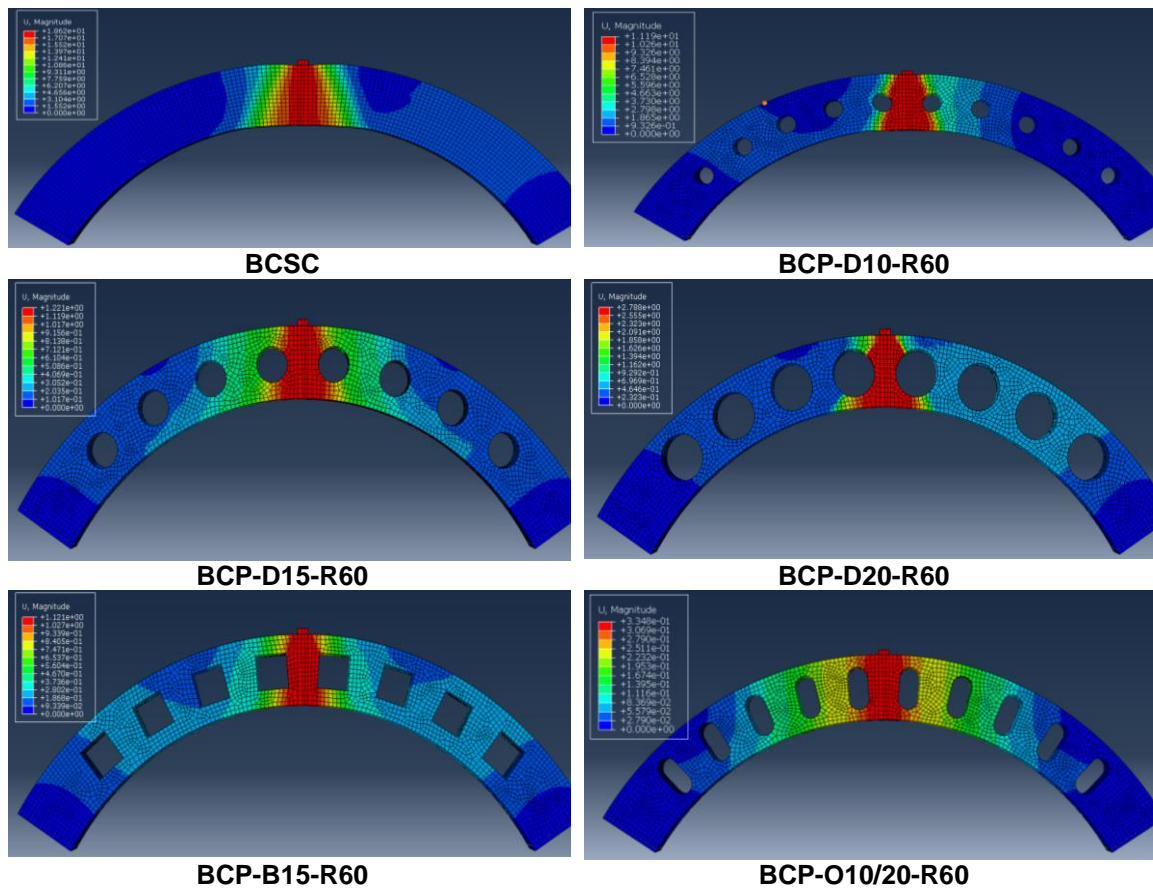

BCSC   **BCP-D10-R60**

BCP-D15-R60   **BCP-D20-R60**

BCP-B15-R60   **BCP-O10/20-R60**

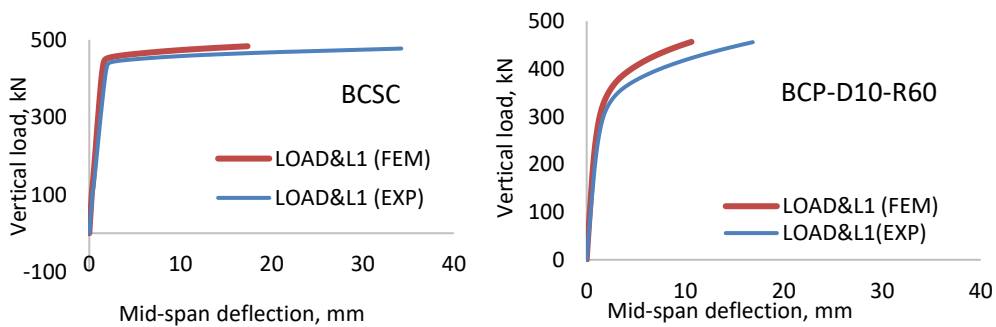**Fig. 12 Modes of failure of tested beams based on numerical simulation.**

Fig. 13(a) Comparison between experimental and numerical results of the load-deflection response for BCSC and BCP-D10-R60.
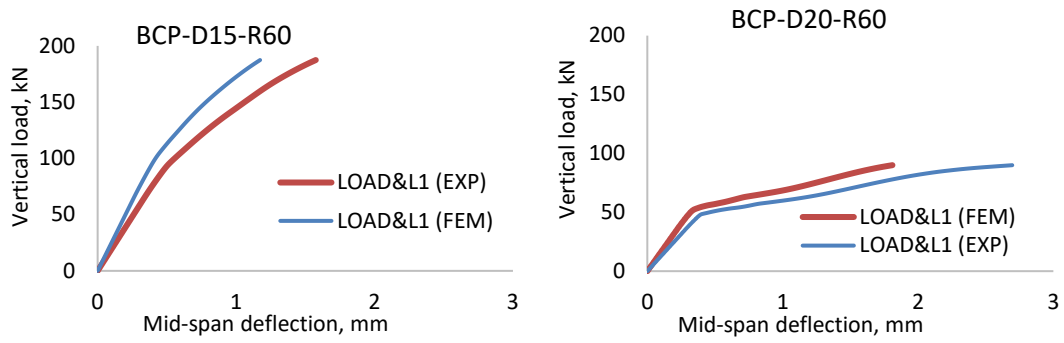
Fig. 13(b) Comparison between experimental and numerical results of the load-deflection response for BCP-D15-R60 and BCP-D20-R60.
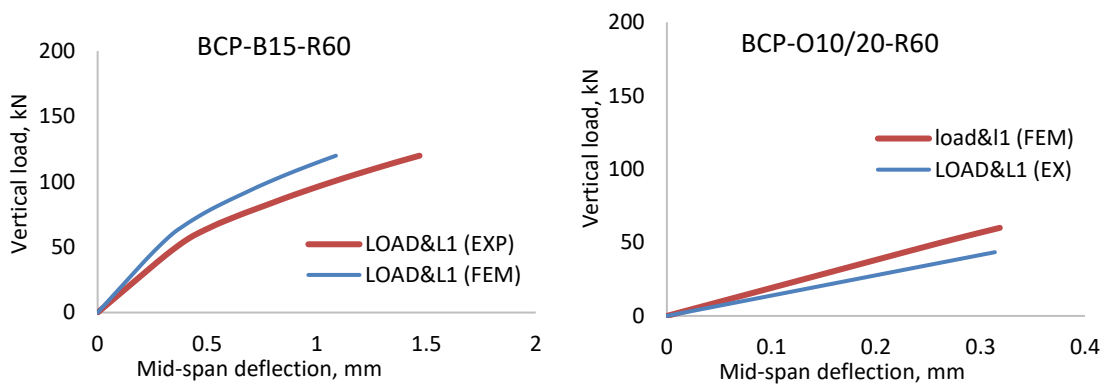

Fig. 13(c) Comparison between experimental and numerical results of the load-deflection response for BCP-B15-R60 and BCP-O10/20-R60.
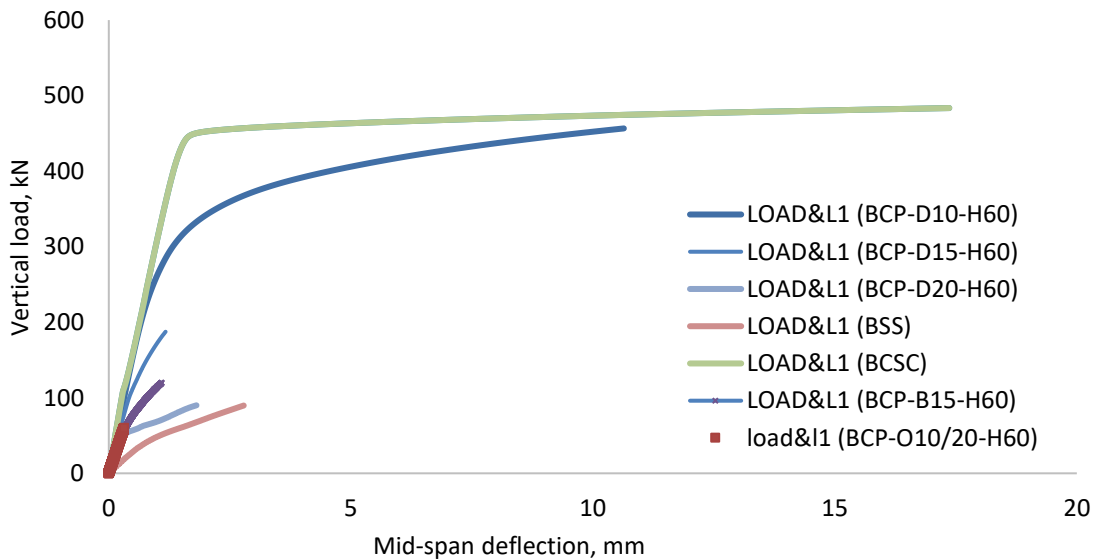

Fig.14 Comparison between all beam tested of the load-deflection response for BSS, BCSC, BCP-D10-R60, BCP-D15-R60, BCP-D20-R60, BCP-B15-R60 and BCP-O10/20-R60.

5. CONCLUSION

Based on the adopted concrete dimensions as well as the reinforcement detailing of the tested beam taking into account the loading scheme, the size and shape of the perforation, the end-conditions and concrete strength and type, the following conclusions maybe drawn:

1. Using curved beam with to mid-span rise to total depth ratio of about 0.27 resulted in hindering the appearance of flexural and shear cracks and increase the ultimate capacity by more than 4 times relative to straight beam. However, the mode of failure maybe switched from flexural to shear mode of failure.

2. Providing multiple perforations of diameter 100 mm ($D/t = 0.33$) in the arched beam showed small decrease in the ultimate capacity of about 6% compared to that of the solid beam. Increasing the perforation size to have 150 mm diameter ($D/t=0.5$) resulted in significant reduction in the ultimate capacity by about 61% compared to that of the solid arched beam; however the ultimate capacity still higher than that of the straight solid beam by about 91%. On contrary, increasing the perforation size further to have D/t of 0.67 resulted in substantial reductions in the ultimate capacity of the ached beam to be in the same order of the straight solid one.

3. For the same mass loss ($D/t=0.5$), circular perforation developed higher ultimate capacity than that developed by square perforations where the ratio between the corresponding capacity was about 1.57.

4. The worst shape of perforation was the oval one where the ultimate capacity decreased below that of the solid straight beam by about 35%.

5. Comparison between numerical simulation and the experimental results showed good agreement from the viewpoint of the displayed mode of failure, ultimate capacity and the developed mid-span deflection relationship.

REFERENCES

[1] Daniel JJ, Revathy DJ. Experimental investigation on flexural strength of beams with opening. Int J Res Manage Tech (IJRMT) 2014; 4:141–3.

[2] Soroush RM, Pabarja AA. The study of the effects of web openings on the concrete beams. Aust J Basic Appl Sci 2011; 5:547–56.

[3] Mansur MA, Tan KH, Lee SL. Collapse loads of RC beams with large openings. ASCE J Struct Eng 1984; 110(11):2602–10.

[4] Prentzas EG. Behavior and reinforcement of concrete beams with large rectangular apertures [Ph.D. thesis]. UK: University of Sheffield; 1968. p. 230.

[5] Al-Sheikh SA. Flexural behavior of RC beams with opening. Concr Res Lett 2014; 5:812–24.

[6] Mansur MA. Effect of openings on the behavior and strength of R/C beams in shear. Cem Concr Comp 1998; 20:477–86.

[7] Al-Sheikh SA. Flexural behavior of RC beams with opening. Concr Res Lett 2014; 5:812–24.

[8] Aykac S, Yilmaz MC. Behaviour and strength of RC beams with regular triangular or circular web openings. J Fac Eng Archit Gazi U 2011; 26:711–8.

[9] Saksena NH, Patel PG. Experimental study of reinforced concrete beam with web openings. Int J Adv Eng Res Stud 2013; 2:66–8.

[10] Aykac B, Kalkan I, Aykac S, Egriboz YE. Flexural behavior of RC beams with regular square or circular web openings. Eng Struct 2013; 56:2165–74.

[11] Abdelaziz, Hamdy M. Afefy, Nesreen M. Kassem, (2021) "Moment redistribution in RC castellated beams subjected to external pre-stressing" Structures and Buildings. DOI: 10.1680/jstbu.20.00206.

[12] Abdelaziz Nabil, Hamdy M. Afefy, Nesreen M. Kassem and Salah El-Din F. Taher, (2019), "Experimental and Numerical Investigations on the Flexural Behavior of RC Castellated Beams" International Conference on Advances in Structural and Geotechnical Engineering, ICASGE'19, Egypt-Africa: TOGETHER WE CAN CONSTRUCT PROMISING FUTURE, Hurghada, Egypt, 25-28 March.

[13] Abdelaziz Nabil, Hamdy M. Afefy, Nesreen M. Kassem and Salah El-Din F. Taher, (2019), " Effect of Openings' Configurations on the Stress Concentration Factor of RC Beams under Different Loading Conditions" International Conference on Advances in Structural and Geotechnical Engineering, ICASGE'19, Egypt-Africa: TOGETHER WE CAN CONSTRUCT PROMISING FUTURE, Hurghada, Egypt, 25-28 March.

[14] Hamida Ibrahim, Hamdy M. Afefy, Nesreen M. Kassem and Salah El-Din F. Taher, (2017), "Structural Performance of Self-compacted Concrete Beams with Rectangular Perforations" International Conference on Advances in Structural and Geotechnical Engineering, ICASGE'17, Hurghada, Egypt, 27-30 March.

[15] Samar Gohar, Hamdy M. Afefy, Nesreen M. Kassem and Salah El-Din F. Taher, (2017) "Flexural performance of self-compacted perforated concrete beams under repeated loading" Engineering Structures, Vol. 143C, July, pp. 441-454. https://doi.org/10.1016/j.engstruct.2017.04.031

[16] ABAQUS, ABAQUS Theory manual, version 6.12, Hibbitt, Carlsson and Sorenson, Inc., Pawtucket, RI, USA, 2012.

[17] Nagataki S, Fujiwara H. Self-Compacting property of Highly-Flowable concrete. In: Malhotra VM, editor. Second conference on advances in concrete technology, ACI SP-154. American Concrete Institute; 1995. p. 301–4.

[18] Okamura H, Ozawa K. Mix design for self-compacting concrete. Concr Library Jpn Soc Civil Eng 1995:107–20.

[19] Petersson O, Billberg P, Van BK. A model for self-compacting concrete. In: Proceedings of production methods and workability of concrete. London: E & FN Spon; 1996. p. 483–92.

[20] Aggarwal P, Siddique R, Aggarwal Y, Gupta SM. Self-compacting concrete – procedure for mix design. Leonardo Electron J Practices Technol 2008; 12:15–24.

[21] Egyptian code for design and construction of reinforced concrete structures (ECP 203-2018); 2018.

[22] Hillerborg, M. M, and P. P.E, (1976) "Analysis of Crack Formation and Crack Growth in Concrete by Means of Fracture Mechanics and Finite Elements", Journal of Cement and Concrete Research, Vol. 6, No. 6, pp. 73-87.

[23] Park H, Paulay T. Reinforced concrete structures. New York: John Wiley and Sons; 1975.